Theory of traffic jam in a one-lane model

Hisao Hayakawa[1,*] and Ken Nakanishi[2,†]
[1]*Graduate School of Human and Environmental Studies, Kyoto University, Kyoto 606-8501, Japan*
[2]*Department of Mechanical Engineering, Shizuoka University, Hamamatsu 432, Japan*
(Received 6 June 1997; revised manuscript received 25 November 1997)

We propose a generalized optimal velocity model to describe one-lane traffic flows. We carry out a weakly nonlinear analysis based on the technique of soliton perturbations and determine the selected propagating velocity, amplitude, and width of the interface between a jam state and a nonjam state. From the direct simulation of the model, we have confirmed the validity of our theoretical analysis. [S1063-651X(98)00204-9]

PACS number(s): 05.20.−y, 47.54.+r, 46.10.+z, 47.20.Ky

I. INTRODUCTION

Recently, the cooperative dynamics in dissipative systems consisting of discrete elements has attracted much attention. There has been research on granular materials in an effort to understand the unusual behaviors of discrete element systems [1] such as convection [2], size segregation [3], bubbling [4], standing waves [5], and localized excitations [6] as well as thermodynamic descriptions of granular particles under vertical vibrations [7]. In particular, it is interesting that flows of granular particles through a vertical pipe can exhibit some interesting characteristics of discrete element systems such as the formation of density waves and a power law in the power spectrum. Similarly, traffic jams in a highway also are an attractive subject for not only engineers but also physicists [8]. Similarities between the two phenomena are obvious. Both consist of discrete dissipative elements, vehicles, and particles that are confined in a quasi-one-dimensional system such as a highway or a pipe. There is an optimal velocity in each system: The competition between relaxation to the optimal velocity and acceleration of particles produces traffic jams. We thus expect that there exists a common and universal mathematical structure behind these phenomena.

There are many models to describe traffic flows and granular flows through a pipe. We believe that universal behaviors do not depend on the choice of the model. We propose here a simple generalized optimal velocity model for traffic flows

$$\ddot{x}_n = a[U(x_{n+1}-x_n)V(x_n-x_{n-1})-\dot{x}_n], \tag{1}$$

where x_n is the position of the nth car and a is a constant called *sensitivity*, which is a parameter to represent driver's response. This model contains the psychological effect of drivers. Namely, the driver of x_n takes care of not only the distance ahead $x_{n+1}-x_n$ but also the distance behind x_n-x_{n-1}. The optimal velocity function U should be a monotonically increasing function of the distance of $x_{n+1}-x_n$ and V should be a monotonically decreasing function of x_n-x_{n-1}. Thus we adopt

$$U(h)=\tanh(h-2)+\tanh(2),$$

$$V(h)=1+f_0[1-\tanh(h-2)] \tag{2}$$

for the latter explicit calculation, where f_0 is a constant. We put these optimal velocity functions as the product form UV in Eq. (1) because the driver of x_n cannot accelerate the vehicle without enough forward distance $x_{n+1}-x_n$ even when the distance x_n-x_{n-1} becomes short. In other words, the model including $U(x_{n+1}-x_n)+V(x_n-x_{n-1})$ is mathematically unstable and unphysical because the acceleration by V causes a crash of vehicles. This model (1) with Eq. (2) is a generalization of the optimal velocity (OV) model proposed by Bando *et al.* [9]

$$\ddot{x}_n = a[U(x_{n+1}-x_n)-\dot{x}_n]. \tag{3}$$

Our model is also similar to the model of granular flow in a one-dimensional tube

$$\ddot{x}_n = \zeta[\tilde{U}(x_{n+1}-x_{n-1})-\dot{x}_n]+\varphi(x_{n+1}-x_n)-\varphi(x_n-x_{n-1}), \tag{4}$$

where $\tilde{U}$ and φ are the sedimentation rate and soft-core repulsion force, respectively [10]. The explicit forms of $\tilde{U}$ and the force φ are not important in our argument. Although real systems contain a variety of vehicles or particles and higher-dimensional effects, we believe that the most essential parts of both traffic flows and granular flows through a pipe can be understood by pure one-dimensional models (1) and (4).

There is a fluid field model to describe traffic flows [11] that consists of mass-conservation and momentum-conservation laws. This fluid model is similar to fluid models that describe granular flows through a pipe and fluidized beds [12–14] and a mixture of polymers [15]. At first sight fluid models are very different from discrete models such as (1), (3), and (4). However, there is common mathematical structure. The fluid models of granular flows are reduced to the Korteweg–de Vries (KdV) equation near the neutral curve of the linear stability [13,14]. Kurtze and Hong [16] also derived the KdV equation from the fluid model of traffic flow [11]. Of course, it is easy to demonstrate that the discrete models (1), (3), and (4) are reduced to the KdV equation near the neutral curve. Thus, at least it has been confirmed that (i) there is a universal mathematical structure

*Electronic address: hisao@phys.h.kyoto-u.ac.jp
†Electronic address: tmknaka@eng.shizuoka.ac.jp

behind traffic flows and granular flows regardless of the choice of a specific model and (ii) solitons perturbed by dissipative corrections play an important role.

Unfortunately, the KdV equation is not adequate to describe traffic jams because its solutions do not contain any interface solutions connecting the jam state and the nonjam state. Komatsu and Sasa [17] solved such a puzzle from the analysis of the original OV model (3). They have shown that Eq. (3) can be reduced to the modified KdV (MKdV) equation at a critical point for the heteroclinic bifurcation [18] or the most unstable point on the neutral curve. They also show that symmetric kink solitons deformed by dissipative corrections describe a separation between bistable states. This analysis is also consistent with a recent analysis of the exactly solvable models, which may be regarded as simplified optimal velocity models [19]. However, as will be shown, the generalized optimal velocity model (1) and the granular model (4) as well as the fluid model of traffic flows [11] and fluid models in granular flows [13,14] are not reduced to the MKdV equation at the critical point or the most unstable point on the neutral curve. In particular, Komatsu [20] has shown that (i) interfaces (kinks) between the jam state and the nonjam state are asymmetric, (ii) the critical point is, in general, different from the most unstable point on the neutral curve, and (iii) eventually one branch of the coexistence curve exists in the linearly unstable region. He also demonstrated that the MKdV equation is recovered in a special choice of parameters of the fluid model, while fluid models cannot be reduced to the MKdV equation in general cases. Thus we need to clarify the characteristics of the dissipative particle dynamics, which contains models (1) and (4) and fluid models [11,13,14]. For this purpose, we will focus on the analysis of the simplest model (1) to characterize the separation between the jam state and the nonjam state because the time needed to simulate model (1) is much shorter than that for fluid models.

This paper is organized as follows. In the next section we briefly summarize the result of the linear stability analysis on the uniform solution of Eq. (1). In Sec. III we derive a steadily propagating solution and discuss the selection of the propagating velocity, the amplitude, and the width of kinks. To demonstrate the quantitative validity of our analysis we will compare it with the result of our simulation in Sec. IV. After the completion of our analysis of Eq. (1), we will briefly discuss the relation of the result and the expected results in Eq. (4) and fluid models in Sec. V. We will summarize the results in Sec. VI.

II. LINEAR STABILITY OF UNIFORM FLOW

In this section we summarize the linear stability analysis of the uniform propagating flow. It is obvious that there is a constant propagating solution with $x_{n+1}-x_n=\text{const}$. Let us rewrite Eq. (1) as

$$\ddot{r}_n=a[U(h+r_{n+1})V(h+r_n)-U(h+r_n)V(h+r_{n-1})-\dot{r}_n], \tag{5}$$

where h is the average distance of successive cars and r_n is $x_{n+1}-x_n-h$. The linearized equation (5) around $r_n(t)=0$ is given by

$$\ddot{r}_n=a[U'(h)V(h)(r_{n+1}-r_n)+U(h)V'(h)(r_n-r_{n-1})-r_n], \tag{6}$$

where the prime refers to the differentiation with respect to the argument. With the aid of the Fourier transformation

$$r_q(t)=\frac{1}{N}\sum_{n=1}^{N}\exp[-iqnh]r_n(t), \tag{7}$$

with $q=2\pi m/Nh$ and the total number of cars N, we can rewrite Eq. (6) as

$$[\partial_t-\sigma_+(q)][\partial_t-\sigma_-(q)]r_q(t)=0, \tag{8}$$

with

$$\sigma_\pm(q)=-\frac{a}{2}\pm\sqrt{(a/2)^2-aD_h[U,V][1-\cos(qh)]+ia(UV)'\sin(qh)}, \tag{9}$$

where we drop the argument h in U and V. $D_h[U,V]\equiv U'(h)V(h)-U(h)V'(h)$ denotes Hirota's derivative. The solution of the initial value problem (8) is the linear combination of terms in proportion to $\exp[\sigma_+(q)t]$ and $\exp[\sigma_-(q)t]$. The mode proportional to $\exp[\sigma_-(q)t]$ can be interpreted as the fast decaying mode, while the term proportional to $\exp[\sigma_+(q)t]$ is the slow and more important mode.

The violation of the linear stability of the uniform solution (6) is equivalent to $\mathrm{Re}[\sigma_+(q)]\geqslant 0$ where $\mathrm{Re}[\sigma_+]$ is the real part of σ_+. Assuming $qh\neq 0$ ($qh=0$ is the neutral mode), the instability condition is given by

$$2(UV)'^2\cos^2\left(\frac{qh}{2}\right)\geqslant aD_h[U,V]. \tag{10}$$

Thus the most unstable mode exists at $qh\to 0$ and the neutral curve for long-wavelength instability is given by

$$a=a_n(h)\equiv\frac{2(UV)'^2}{D_h[U,V]}. \tag{11}$$

The neutral curve in the parameter space (a,h) is shown in Fig. 1 for $f_0=1/[1+\tanh(2)]$ in Eq. (2). For later conve-

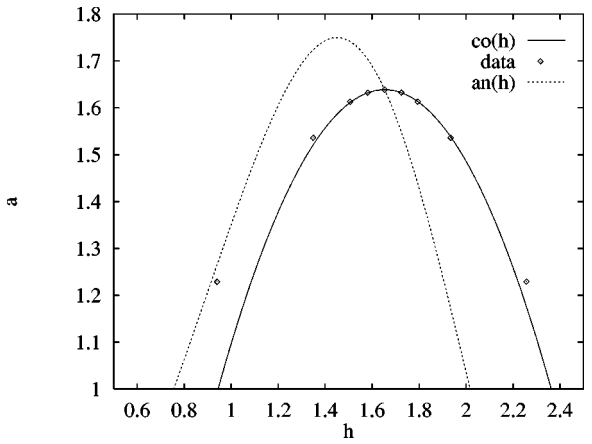

FIG. 1. Plots of the coexistence curve (43) [the solid line denoted by co(h)] and the neutral curve (11) [the dashed line denoted by an(h)] as functions of h. The scattered points are the maximum and the minimum distances of successive cars for a given a obtained from our simulation.

nience we write the explicit form of the long-wavelength expansion of σ_+ in the vicinity of the neutral curve

$$\sigma_+(q)=ic_0qh-c_0^2\frac{a-a_n(h)}{a_n(h)^2}(qh)^2-i\frac{(qh)^3}{6}c_0-\frac{(qh)^4}{4a_n(h)}c_0^2+O((qh)^5), \tag{12}$$

where $c_0=(UV)'$. Thus the uniform state becomes unstable.

III. NONLINEAR ANALYSIS

The simplest way to describe the nonlinear dynamics is the long-wavelength expansion with the help of a suitable scaling ansatz. It is easy to derive the KdV equation near the neutral curve from Eq. (1) as in the case of fluid models [11,13,14]. As mentioned, to describe the traffic jam formation, however, we should choose the critical point $(a,h)=(a_c,h_c)$ at $[U(h)V(h)]''=0$, where the coefficient of $\partial_x r^2$ becomes zero on the neutral curve, because the KdV equation has only pulse solutions while cubic nonlinear terms can produce the interface solution to connect two separated domains. The explicit critical point of Eq. (2) with $f_0=1/[1+\tanh(2)]$ is given by

$$h_c=2-\tanh^{-1}(\tfrac{1}{3})\simeq 1.653\,43; \quad a_c=\tfrac{512}{81}f_0^2\simeq 1.638\,66. \tag{13}$$

Unfortunately, the reduced equation based on the long-wavelength expansion of our model is an ill-posed equation. In fact, the scaling of variables such as $r_n(t)=\epsilon r(z,\tau)$, $z=\epsilon(n+c_0t)$, and $\tau=\epsilon^3 t$ with $\epsilon=\sqrt{(a_c-a)/a_c}$ leads to

$$\partial_\tau r=a_1\partial_z r^3-a_2\partial_z^3 r+a_3\partial_z^2 r^2 \tag{14}$$

in the lowest order, where a_1, a_2, and a_3 are constants. The solution of Eq. (14) diverges within a finite time. The reason is simple. Its linearized equation around $r=d_0$ is unstable for all scales because the solution with $r-d_0\simeq\exp[ikz+\lambda_k\tau]$ has the growth rate $\mathrm{Re}[\lambda_k]=2k^2a_3d_0$, which is always positive when $a_3d_0>0$. Therefore, the simple long-wavelength expansion adopted by Komatsu and Sasa [17] for Eq. (3) and $a_3=0$ cannot be used in our case.

Of course, this irregularity is from the long-wavelength approximation. The regularity of the original model (1) can be checked easily as follows. Let $x=nh$ be regarded as a continuous variable. From $r(x\pm h,t)=\exp[\pm h\partial_x]r(x,t)$ or the Fourier component $\exp[\pm iqh]$ of the translational operator $\exp[\pm h\partial_x]$, the function of the translational operation in the shortest scale ($qh=\pi$ in the Fourier space) is $r(x\pm h,t)\to -r(x,t)$. Thus our model (5) for $r(x,t)$ in the shortest scale is reduced to

$$\partial_t^2 r=a[W(r)-\partial_t r],$$

$$W(r)\equiv U(h-r)V(h+r)-U(h+r)V(h-r). \tag{15}$$

Substituting Eq. (2) into Eq. (15), it is easy to show $W'(r)=-[\mathrm{sech}^2(h-r-2)+\mathrm{sech}^2(h+r-2)]\{1+f_0[1+\tanh(2)]\}<0$. Then the growth rate of the linearized equation (15) by $r-d_0\sim\exp[\lambda t+ikx]$ is given by

$$\lambda=\frac{-a\pm\sqrt{a^2-4a|W'(d_0)|}}{2}, \tag{16}$$

where $\mathrm{Re}[\lambda]\leqslant 0$ for any d_0. Thus the original model (1) is stable for the perturbation in the short scale.

The short scale instability in Eq. (14) thus arises from the insufficiency of the simple long-wavelength expansion. For a theoretical analysis beyond the simple long-wavelength analysis, we have two methods. One is to derive a regularized long-wavelength equation with the help of the Padé approximation [21], which is an interpolation of the short-scale behavior and the long-scale behavior. However, the short-scale analysis of the discrete model contains some subtle problems because of the existence of the cutoff scale. In addition, the reduced partial differential equation is more complicated than the original discrete model (1). Another method is that we focus only on steadily propagating solutions for the theoretical analysis. A dynamical behavior, except for steady states, can be seen from the direct simulation of the discrete model (1), where simulation of model (1) is much easier than the reduced partial differential equations such as the MKdV equation. In addition, our long-time simulation suggests that the solution of model (1) seems to be quickly relaxed to a steadily propagating state. Thus we adopt the latter method for our analysis.

To obtain the steadily propagating kink solution, at first we eliminate the fast decaying mode in Eq. (5) as

$$[\partial_t-\sigma_+(\partial_x)]r(x,t)=(\sigma_+-\sigma_-)^{-1}N[r(x,t)], \tag{17}$$

where $N[r]$ represents the nonlinear terms

$$\frac{N[r]}{a}=U(h+e^{h\partial_x}r(x,t))V(h+r(x,t))-U(h+r(x,t))\times V(h+e^{-h\partial_x}r(x,t))-U'(h)V(h)(e^{h\partial_x}-1)r(x,t)+U(h)V'(h)(1-e^{-h\partial_x})r(x,t). \tag{18}$$

Since $(\sigma_+-\sigma_-)^{-1}$ is the inverse of the polynomial of the differential operators, it is convenient to use the expansion

$(\sigma_+ - \sigma_-)^{-1} \simeq a^{-1}[1-(2h/a)(UV)'\partial_x + O(h^2)]$. It should be noticed that Eq. (17) contains most of the important information and no instability in the time evolution.

Here we assume the scaling of the variables by $\epsilon = \sqrt{(a_c - a)/a_c}$ as

$$r(x,t) = \epsilon \sqrt{\frac{6\gamma c_0}{|(UV)'''|}} R(z), \quad z = \epsilon\sqrt{6\gamma}[n + c_0 t - \epsilon^2 \gamma(t) t], \tag{19}$$

where the arguments in U and V are fixed at $h = h_c$ and γ is the positive free parameter that will be determined from the perturbation analysis. We substitute Eq. (19) into Eq. (17) and expand $N[r]$ as

$$N[r]/a = \sum_{n=1}^{\infty} \sum_{m=2}^{\infty} h^m C_{mn} \partial_x^n r^m - h^3 U' V' \partial_x r \partial_x^2 r + \cdots, \tag{20}$$

where $C_{21} = \frac{1}{2}(UV)''$, $C_{22} = \frac{1}{4} D_h[U,V]'$, $C_{23} = \frac{1}{12}(UV)''$, $C_{31} = \frac{1}{6}(UV)'''$, $C_{32} = \frac{1}{12} D_h[U,V]''$, $C_{41} = \frac{1}{24}(UV)''''$ with $D_h[U,V]' = (d/dh) D_h[U,V]$. Substituting Eq. (19) into Eq. (17) with the help of Eq. (20), we obtain

$$\frac{d}{dz}\left\{ \frac{d^2 R}{dz^2} - R(R^2-1) + \beta \frac{d}{dz}(R^2) \right\} = \epsilon \frac{d}{dz} M[R], \tag{21}$$

where $\beta = 3D_h[U,V]'/(2\sqrt{c_0 |(UV)'''|})$ and

$$M[R] = \sqrt{\gamma}\left[\rho_{23}\left(\frac{dR}{dz}\right)^2 - \rho_{32}\frac{dR^3}{dz} - \rho_{41} R^4 - \frac{1}{4\eta}\left(4\frac{dR}{dz} + \frac{d^3 R}{dz^3} - \frac{2}{\gamma}\frac{dR}{dz} \right) \right] + \dot{\gamma}\left[\frac{zR}{2\gamma^{5/2}} - \gamma t R \right]. \tag{22}$$

Here $\dot{\gamma} = d\gamma/d\tau$ with $\tau = \epsilon t$, and $1/\eta = \sqrt{6} D_h[U,V]/c_0$, $\rho_{23} = 3\sqrt{6} U'V'/\sqrt{c_0 |(UV)'''|}$, $\rho_{32} = \sqrt{3/2} D_h[U,V]''/|(UV)'''|$, and $\rho_{41} = \sqrt{3c_0}(UV)''''/2\sqrt{2|(UV)'''|^3}$.

Assuming $R(z) = R_0(z) + \epsilon R_1(z) + \cdots$, we obtain a solution

$$R_0^{(\pm)}(z) = \tanh(\theta_\pm z), \quad \theta_\pm = \frac{\beta \pm \sqrt{\beta^2 + 2}}{2} \tag{23}$$

in the lowest order. This solution represents a kink or an antikink connecting the jam state and the nonjam state. Notice that the solution is not localized and does not satisfy the periodic boundary condition. Therefore, we need a careful treatment of the boundary condition. In fact, our preliminary result [22] suggests that the selected value of γ under the open boundary condition is different from that under the periodic boundary condition.

In this paper we restrict ourselves to the case under the periodic boundary. To satisfy the periodic boundary condition we use

$$R_0(z) \simeq R_0^{(+)}(z - z_+) - 1 + R_0^{(-)}(z - z_-) \tag{24}$$

as an approximate solution of the lowest-order equation (21), where a kink-antikink pair exists at $z = z_+$ and $z = z_-$. Since Eq. (24) is not an exact solution of Eq. (21), there should be an interaction between the kink and the antikink that is an exponential function of the distance between them [22].

Now let us discuss the effect of perturbative terms in Eq. (21). It is known that the perturbation of solitons or the solution including a free parameter becomes unstable except for the solution where the parameter has a special value [17,23–28]. The linearized equation (21) can be reduced to

$$\mathcal{L} R_1 = \frac{d}{dz} M[R_0], \tag{25}$$

where

$$\mathcal{L} = \partial_z^3 + \partial_z - 6R_0 \partial_z R_0 - 3R_0^2 \partial_z + 2\beta \partial_z^2 R_0 + 4\beta \partial_z R_0 \partial_z + 2\beta R_0 \partial_z^2. \tag{26}$$

To obtain a regular behavior of perturbation in $O(\epsilon)$ the perturbed solution should satisfy the solvability condition

$$\left(\Psi_0, \frac{d}{dz} M[R_0] \right) \equiv \lim_{L\to\infty} \int_{-L}^{L} dz \; \Psi_0 \frac{d}{dz} M[R_0] = 0, \tag{27}$$

where $2L = \epsilon N \sqrt{6\gamma}$ and Ψ_0 satisfies

$$\mathcal{L}^\dagger \Psi_0 = 0, \quad \mathcal{L}^\dagger = -\partial_z^3 - \partial_z + 3R_0^2 \partial_z + 2\beta R_0 \partial_z^2. \tag{28}$$

When we adopt Eq. (24) as R_0, Ψ_0 also should satisfy the periodic boundary condition. Thus we assume

$$\Psi_0(z) = \Psi_0^{(+)}(z - z_+) - 1 + \Psi_0^{(-)}(z - z_-), \tag{29}$$

where $\Psi_0^{(\pm)}$ is the solution of Eq. (28) when we replace R_0 by $R_0^{(\pm)}$. Since $\Phi_0 \equiv \partial_z \Psi_0$ satisfies

$$\tilde{\mathcal{L}}^\dagger \Phi_0(z) = 0, \quad \tilde{\mathcal{L}}^\dagger = -\partial_z^2 - 1 + 3R_0^2 + 2\beta R_0 \partial_z, \tag{30}$$

the solution of Eq. (28) can be expressed by

$$\Psi_0^{(\pm)}(z) = \frac{\alpha_\pm}{2} \int_{-z}^{z} dz' (\mathrm{sech}[\theta_\pm z'])^{1/\theta_\pm^2},$$

$$\Psi_0^{(\pm)}(z) = -\Psi_0^{(\pm)}(-z), \tag{31}$$

where we use

$$\Phi_0^{(\pm)}(z) = (\mathrm{sech}[\theta_\pm z])^{1/\theta_\pm^2}. \tag{32}$$

The constant $\alpha_\pm$ in Eq. (31) is determined to satisfy $\Psi_0(\pm\infty) = -1$. Thus we obtain

$$\alpha_\pm = \frac{2\theta_\pm}{I_0^{(\pm)}},$$

$$I_n^{(\pm)} = \int_{-\infty}^{\infty} dx (\mathrm{sech} x)^{1/\theta_\pm^2 + 2n} = \sqrt{\pi} \frac{\Gamma(1/2\theta_\pm^2 + n)}{\Gamma(1/2\theta_\pm^2 + n + 1/2)}, \tag{33}$$

where $\Gamma(x)$ is the Gamma function. It should be noticed that $\Psi_0(z)$ is not a localized function. Therefore, we cannot neglect the boundary effects in the solvability condition (27).

Let us rewrite Eq. (27) as

$$[\Psi_0 M[R_0]]_{-L}^{L}=(\Phi_0(z),M[R_0]) \tag{34}$$

where $[f(z)]_{-L}^{L}=f(L)-f(-L)$. From Eq. (22) it is obvious that the contribution, except for terms proportional to ρ_{41} and zR, is zero on the left-hand side of Eq. (34) under any boundary conditions. Notice that the contribution from the term proportional to tR vanishes because of its symmetry. If we adopt the periodic boundary condition and use Eqs. (24) and (29), the contribution from the term ρ_{41} cancels [29]. Thus the left-hand side of Eq. (34) is reduced to

$$[\Psi_0 M[R_0]]_{-L}^{L}=\frac{\dot{\gamma}}{\gamma^{5/2}}L. \tag{35}$$

On the other hand, the right-hand side of Eq. (34) is the integration of the product of Eqs. (22) and (32).

For simplicity, to obtain the explicit form we assume $f_0=1/[1+\tanh(2)]$ in Eq. (2). In this case the coefficients in Eq. (37) are reduced to $\rho_{23}=-3/2$, $\rho_{32}=-\beta$, $\rho_{41}=-1/4$, $\eta=1/4\beta$, $c_0=2^6 f_0/3^3=1.206\,89$, $\beta=3\sqrt{3}/8\sqrt{2}f_0=0.902\,037$, $6c_0/|(UV)'''|=9/4$, $\theta_+=1.289\,718\,7$, and $\theta_-=-0.387\,814$. Thus we obtain

$$\{L-(\theta_+-\theta_-)\}\dot{\gamma}=4\beta\gamma^2\left\{\frac{\theta_+}{\theta_+^2+1}\left(1-\frac{\gamma}{\gamma_+}\right)-\frac{\theta_-}{\theta_-^2+1}\left(1-\frac{\gamma}{\gamma_-}\right)\right\}, \tag{36}$$

where we use

$$\frac{I_{n+1}^{(\pm)}}{I_n^{(\pm)}}=\frac{2n\theta_\pm^2+1}{(2n+1)\theta_\pm^2+1}.$$

Here $\gamma_\pm$ is given by

$$\gamma_\pm^{-1}=2+\theta_\pm^2\left(2-3\frac{I_2^{(\pm)}}{I_1^{(\pm)}}\right)+2\eta\left[3\rho_{32}\left(1-\frac{I_2^{(\pm)}}{I_1^{(\pm)}}\right)+\frac{\rho_{41}}{\theta_\pm}\left(\frac{I_0^{(\pm)}}{I_1^{(\pm)}}-2+\frac{I_2^{(\pm)}}{I_1^{(\pm)}}\right)-\rho_{23}\theta_\pm\frac{I_2^{(\pm)}}{I_1^{(\pm)}}\right]. \tag{37}$$

Rearrangement of $\gamma_\pm$ leads to

$$\gamma_\pm=\frac{8\beta\theta_\pm(3\theta_\pm^2+1)}{37\theta_\pm^4+8\theta_\pm^2-8}. \tag{38}$$

Substituting Eq. (38) into Eq. (36), we obtain

$$(L-\theta_++\theta_-)\dot{\gamma}=\alpha\gamma^2\left(1-\frac{\gamma}{\gamma^*}\right), \tag{39}$$

where

$$\alpha=\frac{24\beta\sqrt{\beta^2+2}}{4\beta^2+9},\quad \gamma^*=\frac{3(12\beta^2+25)}{61\beta^2+132}=0.574\,189\ldots. \tag{40}$$

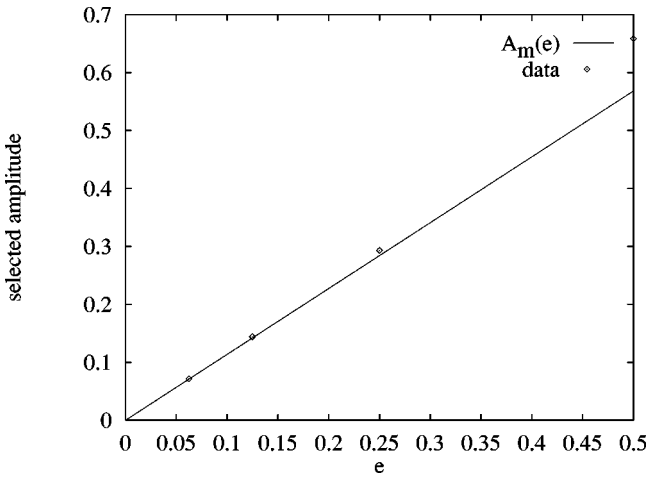

FIG. 2. Comparison of A_m^* between theoretical values [solid line $A_m(e)=1.136\,63\epsilon$] in Eq. (41) and numerical value (data). The horizontal axis e represents ϵ.

From Eq. (19) the amplitude $A\epsilon$ of R_0 can be regarded as the order parameter of phase separation, which is given by

$$A\epsilon\equiv\frac{3}{2}\epsilon\sqrt{\gamma^*}\simeq 1.136\,63\epsilon. \tag{41}$$

In the vicinity of γ^* the time evolution of γ is described by

$$\gamma(\tau)\simeq\gamma^*+[\gamma(0)-\gamma^*]\exp\left[-\frac{\alpha\gamma^*}{L^*}\tau\right], \tag{42}$$

where $L^*=\epsilon N\sqrt{6\gamma^*}$. Notice that γ^* is the stable fixed point in the time evolution (39), where we use $(\theta_+-\theta_-)/L\ll 1$.

Two remarks about the result of this section are addressed. First we recall that to derive Eq. (40) from Eq. (34) we assume that $f_0=1/[1+\tanh(2)]$. Although it is not difficult to obtain the result for any f_0, we omit such a discussion to avoid long and tedious calculations. Second, the characteristic time for the relaxation (39) or (42) is proportional to the system size L. This result is reasonable because the time needed to simulate model (1) is proportional to the number of cars N. This tendency will be confirmed by the simulations in the next section.

IV. SIMULATION

To check the validity of our analysis in the preceding section we perform the numerical simulation of Eqs. (1) and (2) with $f_0=1/[1+\tanh(2)]$ and Eq. (13) under the periodic boundary condition. We adopt the classical fourth-order Runge-Kutta scheme with fixed time interval $\Delta t=2^{-4}$. Since our purpose is the quantitative test of Eqs. (23) and (40), the initial condition is restricted to a symmetric kink-antikink pair. Taking into account the scaling properties, we perform the simulation for the set of parameters $(\epsilon,N)=(1/2,32),(1/4,64),(1/8,128),(1/16,256)$ until r_n relaxes to a steadily propagating state. Our results are plotted in Figs. 1–3. Figure 1 displays the data for maximum h_{max} and minimum h_{min} values of the successive car distance in a steady state obtained from our simulation in each parameter set. The solid line in Fig. 1 is the theoretical coexistence curve

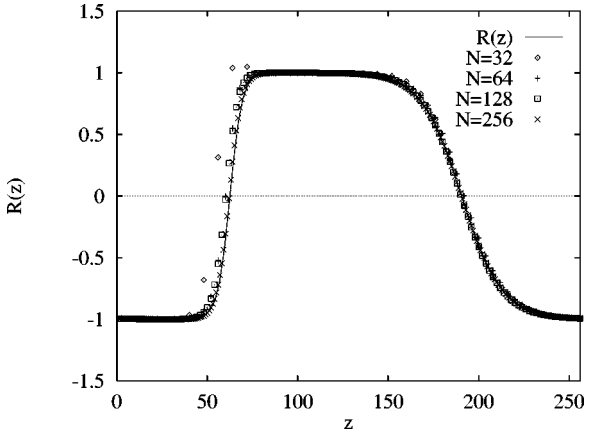

FIG. 3. Linear combination of our theoretical curve (23) and the scaled simulation data of the relative distance of successive cars for $(\epsilon,N)=(1/2,32),(1/4,64),(1/8,128)$, and $(1/16,256)$, where N denotes the scaled data for N-car systems. The solid curve is $R(z)=\tanh[\xi\theta_+(z-z_+)]-1+\tanh[\xi\theta_-(z-z_-)]$, with $\xi=(6\gamma^*)^{1/2}/16$ and two fitting parameters $z_+=62.5$ and $z_-=190.5$, where the spatial scale is measured by the average distance in $N=256$.

$$a=a_c\left(1-\frac{(h-h_c)^2}{A^2}\right), \quad A=1.136\,63\ldots, \tag{43}$$

where we use $a=a_c(1-\epsilon^2)$ and $A\epsilon=h-h_c$. The agreement is obvious. From this figure we can see that one of the branches is in the linearly unstable region, but the theoretical curve recovers the simulation result. Figure 2 is the direct comparison between the theoretical amplitude (41) and the result of simulation, where the data point is $A_m^*\equiv(h_{max}-h_{min})/2$. We stress that the evaluated value of A from simulation at $\epsilon=1/16$ is $1.142\,73\ldots$. Thus the deviation between simulation and theory is only 0.53%.

Figure 3 demonstrates that the numerical result has a scaling solution that has an asymmetric kink-antikink pair. The linear combination of our theoretical curve (23) and Eq. (38) is plotted as the solid line by choosing the position of the kink and the antikink. Our theoretical curve agrees with the simulation value without other fitting parameters. Thus we have confirmed the validity of our theoretical analysis in steady states.

Figure 4 displays the time evolution of the kink amplitude $A_m(t)=[h_{max}(t)-h_{min}(t)]/2$ for several system sizes of the simulation of the original OV model (3) at $\epsilon=1/8$ and $h=2$. The data suggest that the exponential time evolution in Eq. (42) seems to be valid even in relatively early stages. It is obvious that the characteristic time for the relaxation to A_m^* can be scaled by N. The solid line represents the theoretical prediction, where Eq. (42) in this case is reduced to $f(t/N)=\exp[-(8/3)\sqrt{2\gamma^*}\epsilon^3 t/N]$ with $\gamma^*=5/4$. The agreement between the theoretical curve and our numerical result is fairly good. Thus the validity of the time evolution (42) has been confirmed by the simulation.

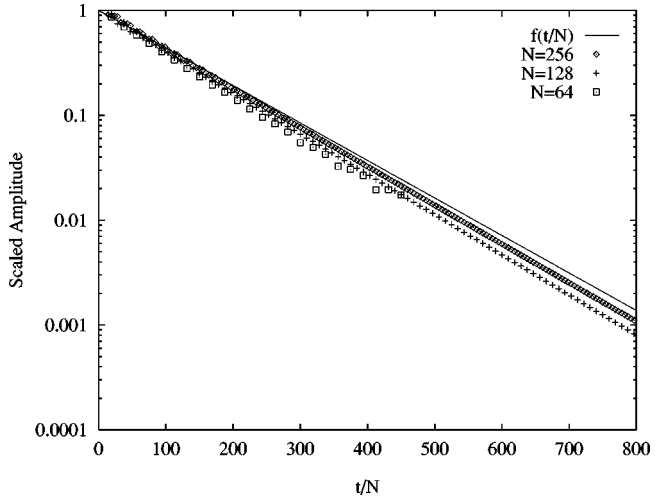

FIG. 4. Semilogarithmic plots of $A_m(t)$ with the original optimal velocity model (3) for several system sizes: $N=64$, 128, and 256, where N is the number of cars. The vertical axis denotes the scaled amplitude $[A_m(t)-A_m^*]/[A_m(0)-A_m^*]$, where the selected amplitude A_m^* is obtained from an average of the last 10 data points, where γ^* is determined from the average of the last 20 data points. The horizontal axis is the normalized time t/N. The conditions of the simulation are $\epsilon=1/8$, $h=2$, and $\Delta t=2^{-4}$. The solid line represents $f(t/N)$ in the text.

V. DISCUSSION

As we have seen in the previous sections, our theoretical analysis gives very precise results for the separation between jam states and nonjam states. Of course, we do not think that our analysis is perfect. Since, for example, we omit the time evolution of reduced dynamical models, we cannot explain the reason why the branch in a linearly unstable state is stable in our simulation (see Fig. 1). The mechanism for stabilizing the branch should be explained in terms of a simple physical picture. The validity of the choice of Eqs. (24) and (29) is not confirmed from a mathematical point of view, although this choice works very well. Clarification of the above points will be a subject of our future research.

Let us comment on the universality class of traffic flows and granular flows. All the models introduced here, except for model (3), have asymmetric kink-antikink pairs and have qualitatively similar behaviors. Komatsu [20] has derived Eq. (14) as the long-wavelength equation from the fluid model of traffic flow [11]. It is also easy to derive Eq. (14) from Eq. (4) and fluid models for granular flows. In this sense, granular flows through a pipe and traffic flows compose a universality class and our discussion here essentially can be used in any models for traffic flows and granular flows. In fact, we [30] have already checked the quantitative validity of our methods presented here for the fluid model in traffic flows [11]. On the other hand, the OV model (3) is a special case of the above generalized models. For example, the models with $f_0=0$ [Eq. (2)] and $\tilde{U}''(h_c)=0$ [Eq. (4)] are reduced to the MKdV equation. Namely, the behaviors in the original OV model are not universal in models for one-dimensional dissipative flows. It should be noticed that the limitation of the OV model has been suggested by Komatsu and Sasa (see the last part in Ref. [17]). Therefore, we believe that our analysis is important in the characterization of the universal feature of one-dimensional dissipative flows such as granular flows through a pipe and traffic flows.

In realistic situations, highways have multiple lanes and vehicles can pass slow vehicles. When we include multilane

effects in one-dimensional models, the separations between jam states and nonjam states become obscured. However, there is another universal law in quasi-one-dimensional systems for dissipative discrete element flows, i.e., a power law in the power spectrum. Recently, it has been shown [10,31] that both models (1) and (4) supplemented by the white noise produces a power law in the frequency spectrum of the density $P(f) \sim f^{-4/3}$ numerically and analytically, whose exponent $-4/3$ is very close to the experimental value [10] and the value from the lattice-gas automata simulation [32]. From this success the essential effects of randomness such as passing vehicles and a variety of vehicles seem to be represented by the addition of white noise to the models (1) and (4) [33]. In this sense, again, we believe that the fundamental research on pure one-dimensional models is meaningful. The details of the analysis of the added noise models for dissipative particles flows will be discussed elsewhere.

VI. CONCLUSION

In conclusion, we have proposed a simple generalized optimal velocity model (1). Based on the perturbation analysis of asymmetric kink solution (23) we obtain the selected values of its amplitude, propagating velocity, and width of kink as in (40). The accuracy and relevancy of the solution has been confirmed by the direct simulation.

ACKNOWLEDGMENTS

H.H. thanks Ooshida T. and S. Wada for fruitful discussion. This work was partially supported by a Grant-in-Aid from the Ministry of Education, Science and Culture of Japan (Grant No. 09740314).

[1] H. Hayakawa, H. Nishimori, S. Sasa, and Y.-h. Taguchi, Jpn. J. Appl. Phys., Part 1 **34**, 397 (1995); H.M. Jaeger, S.R. Nagel, and R.B. Behringer, Rev. Mod. Phys. **68**, 1259 (1996), and references therein.

[2] Y.-h. Taguchi, Phys. Rev. Lett. **69**, 1367 (1992); H. Hayakawa, S. Yue, and D. C. Hong, *ibid.* **75**, 2328 (1995); K. M. Aoki, T. Akiyama, Y. Maki, and T. Watanabe, Phys. Rev. E **54**, 874 (1996).

[3] A. Rosato, K. J. Strandburg, F. Prinz, and R. H. Swendsen, Phys. Rev. Lett. **58**, 1038 (1987).

[4] H. K. Pak and R. P. Behringer, Nature (London) **371**, 231 (1994).

[5] F. Melo, P. B. Umbanhowar, and H. L. Swinney, Phys. Rev. Lett. **75**, 3838 (1995).

[6] P. B. Umbanhowar, F. Melo, and H. L. Swinney, Nature (London) **382**, 793 (1996).

[7] See, e.g., H. Hayakawa and D. C. Hong, Phys. Rev. Lett. **78**, 2764 (1997).

[8] See, e.g., G. B. Whitham, *Linear and Nonlinear Waves* (Wiley, New York, 1974); R. Huberman, *Mathematical Model: Traffic Flow* (Prentice Hall, Englewood Cliffs, NJ, 1977); D. Helbing, *Traffic Dynamics: New Physical Modeling Concepts* (Springer, Berlin, 1997).

[9] M. Bando, K. Hasebe, A. Nakayama, A. Shibata, and A. Sugiyama, Phys. Rev. E **51**, 1035 (1995).

[10] O. Moriyama, N. Kuroiwa, M. Matsushita, and H. Hayakawa (unpublished).

[11] B.S. Kerner and P. Konhauser, Phys. Rev. E **48**, 2335 (1993).

[12] G.K. Batchelor, J. Fluid Mech. **193**, 75 (1988).

[13] S. Sasa and H. Hayakawa, Europhys. Lett. **17**, 685 (1992); T. S. Komatsu and H. Hayakawa, Phys. Lett. A **183**, 56 (1993).

[14] M. F. Göz, Phys. Rev. E **52**, 3697 (1995).

[15] M. Doi and A. Onuki, J. Phys. II **2**, 1631 (1992).

[16] D. A. Kurtze and D. C. Hong, Phys. Rev. E **52**, 218 (1995).

[17] T. S. Komatsu and S. Sasa, Phys. Rev. E **52**, 5574 (1995).

[18] More precisely, the critical point on the neutral curve is the bifurcation point from a homoclinic solution (trajectory to connect one stable point) such as KdV pulses to a heteroclinic solution (trajectory to connect two stable points) such as MKdV kinks.

[19] Y. Sugiyama and H. Yamada, Phys. Rev. E **55**, 7749 (1997); K. Nakanishi, K. Itoh, Y. Igarashi, and M. Bando, *ibid.* **55**, 6519 (1997).

[20] T. S. Komatsu, Ph.D. thesis, Tohoku University, 1996 (unpublished).

[21] Ooshida T. and T. Kawahara, Phys. Rev. E **56**, 511 (1997).

[22] K. Nakanishi and H. Hayakawa (unpublished).

[23] E. J. Hinch, *Perturbation Methods* (Cambridge University Press, Cambridge, 1991).

[24] E. Ott and R. N. Sudan, Phys. Fluids **12**, 2388 (1969).

[25] Y. S. Kivshar and B. A. Malomed, Rev. Mod. Phys. **61**, 763 (1989).

[26] H. Hayakawa [Theor. Math. Phys. **99**, 309, (1994).]

[27] S. Ei and T. Ohta, Phys. Rev. E **50**, 4672 (1994).

[28] L. Y. Chen, N. Goldenfeld, and Y. Oono, Phys. Rev. E **54**, 376 (1996).

[29] In other words, the contribution from the term ρ_{41} exists if the system is under the free boundary condition [22].

[30] S. Wada and H. Hayakawa, J. Phys. Soc. Jpn. (to be published).

[31] H. Hayakawa and K. Nakanishi, Prog. Theor. Phys. Suppl. (to be published).

[32] G. Peng and H. J. Herrmann, Phys. Rev. E **49**, 1796 (1994); **52**, 5597 (1995).

[33] It should be noted that to obtain the exponent $-4/3$ requires a well-controlled experiment about air flow. Thus, early experiments without controll of the air flow reported slightly larger values of the exponent, e.g., -1.5 rather than $-4/3$. See, e.g., the earlier papers of S. Horikawa, A. Nakahara, T. Nakayama, and M. Matsushita, J. Phys. Soc. Jpn. **64**, 1870 (1995); S. Horikawa, T. Isoda, T. Nakayama, A. Nakahara, and M. Matsushita, Physica A **233**, 699 (1996), where they have refined the experimental setup and concluded 4/3 in their recent paper [10].